J. Fluid Mech. (2002), *vol.* 467, *pp.* 389–410.
DOI: 10.1017/S0022112002001532 Printed in the United Kingdom

Viscous interactions of two co-rotating vortices before merging

By STÉPHANE LE DIZÈS AND ALBERTO VERGA

Institut de Recherche sur les Phénomènes Hors Équilibre (IRPHE), 49, rue F. Joliot Curie, BP 146, F-13384 Marseille cedex 13, France

(Received 1 October 2001 and in revised form 20 February 2002)

The viscous evolution of two co-rotating vortices is analysed using direct two-dimensional numerical simulations of the Navier–Stokes equations. The article focuses on vortex interaction regimes before merging. Two parameters are varied: a steepness parameter n which measures the steepness of the initial vorticity profiles in a given family of profiles, and the Reynolds number Re (between 500 and 16 000). Two distinct relaxation processes are identified. The first one is non-viscous and corresponds to a rapid adaptation of each vortex to the external (strain) field generated by the other vortex. This adaptation process, which is profile dependent, is described and explained using the damped Kelvin modes of each vortex. The second relaxation process is a slow diffusion phenomenon. It is similar to the relaxation of any non-Gaussian axisymmetrical vortex towards the Gaussian. The quasi-stationary solution evolves on a viscous-time scale toward a single attractive solution which corresponds to the evolution from two initially Gaussian vortices. The attractive solution is analysed in detail up to the merging threshold $a/b \approx 0.22$ where a and b are the vortex radius and the separation distance respectively. The vortex core deformations are quantified and compared to those induced by a single vortex in a rotating strain field. A good agreement with the asymptotic predictions is demonstrated for the eccentricity of vortex core streamlines. A weak anomalous Reynolds number dependence of the solution is also identified. This dependence is attributed to the advection–diffusion of vorticity towards the hyperbolic points of the system and across the separatrix connecting these points. A $Re^{1/3}$ scaling for the vorticity at the central hyperbolic point is obtained. These findings are discussed in the context of a vortex merging criterion.

1. Introduction

Since the pioneering experiments carried out by Couder (1983) on two-dimensional turbulence in thin films, it has been clear that vortex interactions, and in particular vortex merging, are essential processes which ultimately determine the flow behaviour. Couder (1983) found that the mean vortex size grows with time in qualitative agreement with the theoretical prediction of the 'inverse cascade'. The direct observation of coherent structures, already present in early numerical simulations (Basdevant *et al.* 1981), inspired further investigations on this subject. Later, many works were devoted to the study of the evolution of a random distribution of vorticity, especially using numerical simulations (McWilliams 1984, 1990). In decaying turbulence, vortex merger can be considered as the most important interaction, although other multiple vortex collisions or inelastic encounters influence the system's evolution (Dritschel

1995; Kevlahan & Farge 1997). A scaling theory of two-dimensional turbulence was proposed by Carnevale *et al.* (1991, 1992), based on the pathway of successive generations of vortices.

Vortex merger is also important in a variety of fluid flows, such as in mixing layers (Winant & Browand 1974) or aircraft wakes (Brandt & Iversen 1977). In order to understand the merging mechanism a variety of simplified models were investigated: models where viscous effects are neglected, and only the vortex core evolution is considered as in the case of vortex patches (Saffman & Szeto 1980) or vorticity contour dynamics (Dritschel & Waugh 1992); models with the opposite approximation, where vortex core size is neglected and viscous effects control the vortex interaction (Agullo & Verga 2001). Overman & Zabusky (1982), using contour dynamics, studied the instability, merger and breaking of two patches of vorticity, and tested the merger criterion (Saffman 1992). This criterion stipulates that merging of two identical vortices is only possible if the ratio of the vortex size to their separation is larger than a certain threshold. In fact, when dissipation is taken into account, the vortex size grows in time and vortex merging always occurs, whatever is the initial condition, as noted by Melander, Zabusky & McWilliams (1988). Interestingly, even in the extreme case of point vortices, viscosity also drives vortices to merge in a finite time as demonstrated by the stochastic approach of Agullo & Verga (2001). Melander *et al.* (1988) simulated, using hyperviscosity as a dissipation process, the interaction of two vortices having a continuous vorticity distribution (initially of compact support). The results of the direct simulations were compared with a simple dynamical model derived from a truncation of the Navier–Stokes equation to the second moments of the vorticity. This reduced dynamical system, which incorporates viscous effects, has its own merging process. One important observation of Melander *et al.* (1988) was that the merging process includes different stages. After an initial 'adaptation' stage, the system sets into a metastable state, which evolves slowly on a viscous time scale up to a 'critical' state from which merger occurs on a convective time scale. This scenario was qualitatively confirmed by their numerical simulations. However the model, which did not take into account the emergence of the spiral structure and the overlapping of vorticity, could not reproduce the successive stages with the correct time scales. Here, both the adaptation stage and the 'metastable' state are analysed in detail using real viscous diffusion and overlapping vorticity profiles.

The existence of an attracting metastable state was also noted in the recent work of Sipp, Jacquin & Cossu (2000), where they study the self-adaptation and viscous selection of two counter-rotating vortices (in two dimensions). The metastable state appears to be very close to a solution of the Euler equations, adiabatically evolving by viscous diffusion. In the case of co-rotating vortices, experiments carried on by Meunier & Leweke (2001) also show the existence of a quasi-steady state, where the distance between the two vortices remains almost constant and the rotation period is near that of two point vortices with equivalent circulation. This quasi-steady state was compared to equilibrium solutions of Euler equations (Ehrenstein & Rossi 1999; Meunier *et al.* 2002) in order to establish a merging criterion based on the stability of the metastable state.

The initial stage of the co-rotating vortices evolution, before important changes arise in the initial vorticity distribution, is dominated by the strain field felt by each vortex due to the action of the other one. This strain field tends to elliptically deform the core of the vortex. Moore & Saffman (1971) first explained this deformation by providing an equilibrium solution for a non-viscous vortex patch in a stationary strain field. Jiménez, Moffatt & Vasco (1996) and Le Dizès (2000) obtained similar

equilibrium solutions for a Gaussian vortex in a weak strain field. The time-dependent adaptation process of the vortex to the strain field has also been the subject of several recent works (Lingevitch & Bernoff 1995; Bassom & Gilbert 1999; Schecter *et al.* 2000; Balmforth, Llewellyn Smith & Young 2001). Bassom & Gilbert (1999) showed that the non-viscous vortex response involves a complex spiral structure which is characterized in the large time limit by a peculiar algebraic decreasing behaviour. Sipp *et al.* (2000) discussed the adaptation process in a system composed of two counter-rotating vortices. They observed that the vortex ellipticity oscillates during the adaptation process. They showed that for vortices with uniform vorticity profiles (Rankine vortices), the oscillations of the core elliptic deformation could be attributed to a linear Kelvin mode. In the present paper, we reach a similar conclusion in the context of co-rotating vortices for other vortices such as the Gaussian vortex. We further demonstrate that the adaptation process is independent of the Reynolds number in agreement with the properties of the Kelvin modes.

The paper is organized as follows. In § 2, the numerical procedure is presented together with the basic properties of a system of two co-rotating vortices. Vortex deformation measures are defined in this section. In § 3, two relaxation processes are identified for sufficiently distant vortices. The rapid vortex core adaptation mentioned above is analysed in § 3.1. Both vorticity profile and Reynolds number are varied to prove the direct relation of this process to a damped deformation mode of each vortex. The second slow relaxation process, which is due to viscous diffusion is described in § 3.2. As for counter-rotating vortices (Sipp *et al.* 2000), the vortex system with a Gaussian initial profile is shown to attract all the other vortex systems with different initial vorticity profiles. We demonstrate that this process is similar to the relaxation of a single axisymmetric vortex to a Gaussian. Properties of the attractive state are provided in §§ 4 and 5. In § 4, the quasi-steady character of the system is demonstrated. The streamline eccentricity near each vortex centre is also shown to be well-predicted by that of a single vortex in a rotating strain field. A weak Reynolds number dependence near the streamlines connected to the hyperbolic points of the system is identified in § 5 in the range $Re = 500$–8000 we consider. The vorticity in the central hyperbolic points is in particular shown to exhibit an unusual $Re^{1/3}$ scaling. Possible physical mechanisms associated with these phenomena are briefly discussed in this section. The last section provides a summary of the main results.

2. Framework

2.1. *Equations and parameters*

The streamfunction Ψ and the vorticity ω are governed by the two-dimensional vorticity equation

$$\frac{\partial \omega}{\partial t} - \mathscr{J}[\Psi, \omega] = \nu \nabla^2 \omega, \tag{2.1a}$$

$$\omega = -\nabla^2 \Psi, \tag{2.1b}$$

where ν is the kinematic viscosity and the Jacobian $\mathscr{J}$ is defined by

$$\mathscr{J}[f, g] = \frac{\partial f}{\partial x}\frac{\partial g}{\partial y} - \frac{\partial f}{\partial y}\frac{\partial g}{\partial x}$$

in Cartesian coordinates (x, y).

We consider the time evolution of two identical vortices which are initially axisymmetrical, of radius $a_0 = a(0)$, circulation Γ and whose centres are separated by a

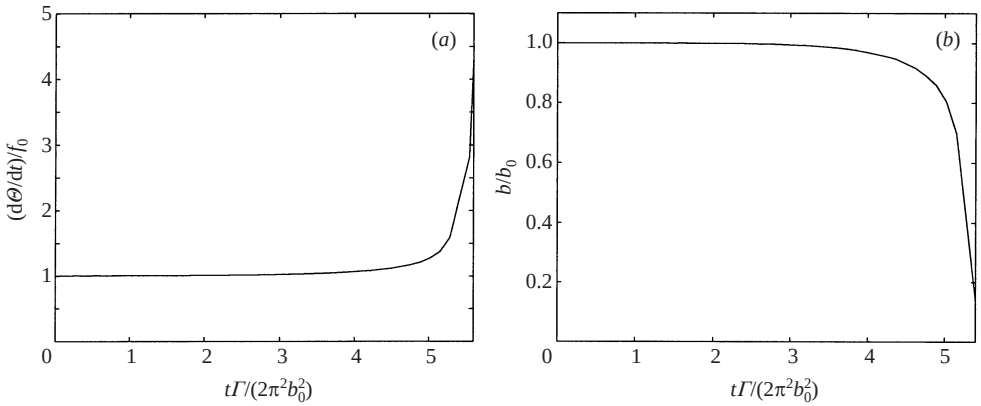

FIGURE 1. Typical evolution of the angular frequency (a) and the separation distance (b) between vortex centroids as a function of time (normalized by the turnover time), for $n = 1$, $a_0/b_0 = 0.05$, $Re = 8000$.

distance $b_0 = b(0)$. Each vortex initially has a profile of the form

$$\omega_0(r) = \exp(-r^{2n}). \tag{2.2}$$

It is parametrized by a single parameter n which measures the steepness of the profile. The profile is Gaussian for $n = 1$ and approximately 'top-hat' for large n. For any n, the non-dimensionalized circulation and radius (which is precisely defined below from the vorticity second-order moment) can be expressed in terms of the Euler's Gamma function $\Gamma(x)$ as

$$a_0^2 = \frac{\Gamma(2/n)}{\Gamma(1/n)}, \tag{2.3a}$$

$$\Gamma = \frac{\pi\Gamma(1/n)}{n}. \tag{2.3b}$$

These values are useful for normalization purposes.

The time-evolution is characterized by three parameters: the steepness parameter n, the initial ratio a_0/b_0 and the Reynolds number $Re = \Gamma/\nu$. Here we consider $n = 0.5, 1, 4$, initial ratio $a_0/b_0 = 0.05, 0.1$, and Reynolds numbers ranging from 500 to 16 000. These Reynolds numbers are large enough to have well-separated viscous and convective time scales.

The simulations are performed in a periodic square box of size $2\pi \times 2\pi$ using spectral methods in a grid of 1024 by 1024 points and second-order time integration. The vortices are initially located on the y-axis at $x = \pm\pi/8$ such that the distance b_0 between the two vortices is eight-times smaller than the length of the box. The simulation was qualified by monitoring the energy. In all simulations the energy balance was satisfied with a relative error smaller than 10^{-6}.

2.2. *Description of the flow*

A first picture of the dynamics of two co-rotating vortices is obtained by assuming that the circulation Γ of each vortex is concentrated in its vortex centroid. In this point-vortex model, the non-viscous dynamics is trivial: the vortices remain separated by a constant distance b_0, and rotate around each other at a constant angular frequency $f_0 = \Gamma/(\pi b_0^2)$. Interestingly, this dynamics is also valid for a finite size vortex. This is illustrated on figure 1(a, b) where typical time-evolutions of both the

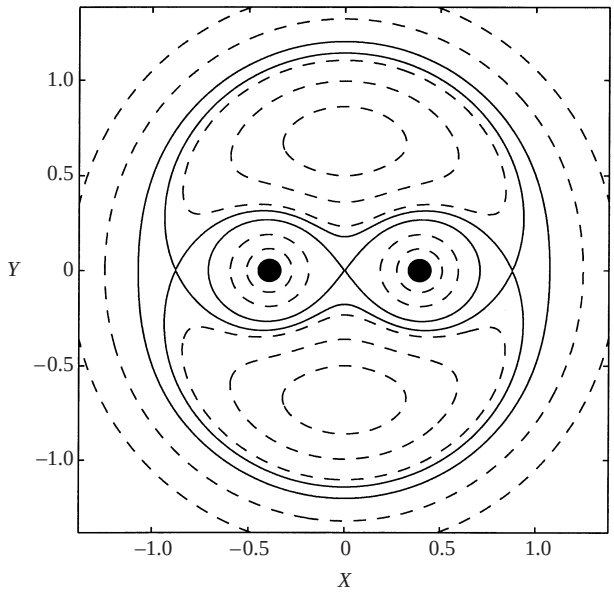

FIGURE 2. Streamlines of two co-rotating vortices in the rotating frame for small a/b. (Here $a/b \approx 0.067$.) The solid lines are separatrices connected to an hyperbolic point of the system. The two vortices are indicated by the black circles. (Their size corresponds to a 50% vorticity level.)

angular frequency f and the separation distance b are displayed. On these plots, f and b are shown to remain constant up to a critical time (here near 5 turnover times), which corresponds to the beginning of merging. In the following, this trivial non-viscous dynamics is removed by considering the evolution of the system in a frame (X, Y) rotating at the angular frequency f. A typical streamline pattern in this rotating frame is shown in figure 2.

Corrections to the 'point-vortex dynamics' are generated by both viscous diffusion and vortex core deformation. The deformation of each vortex core is due to the non-homogeneous velocity field created by the other vortex. It is easy to show that, for small a/b, this 'external' field is at leading order a strain field of strain rate $S_e = \Gamma/(2\pi b^2)$. Such a strain field tends to deform each vortex core into an ellipse (Moore & Saffman 1971). The goal of an important part of the paper is to characterize this deformation. For this purpose, both a global and a local measure of the elliptic deformation are considered.

2.3. *Global and local eccentricities*

The local measure we shall consider is the eccentricity of the streamline near the vortex stagnation point (X_i, Y_i) (in the rotating frame). It is a quantity which has often been used to characterize the deformation of a vortex in an external strain field (Jiménez *et al.* 1996; Le Dizès 2000). It is defined in the following way. If the rotating frame is chosen such that $Y_i = 0$, the two vortices then have their stagnation points at $(\pm X_i, 0)$. Using a Taylor expansion, the streamfunction can be written at leading order near $(X_i, 0)$ as

$$\Psi \sim (\mu_i - S_i)(X(\Theta_i) - X_i)^2 + (\mu_i + S_i)Y(\Theta_i)^2 \tag{2.4}$$

where $X(\Theta_i)$ and $Y(\Theta_i)$ are the coordinates in the frame rotated by an angle Θ_i:

$$X(\Theta_i) = \cos\Theta_i X + \sin\Theta_i Y, \tag{2.5a}$$

$$Y(\Theta_i) = \cos\Theta_i Y - \sin\Theta_i X. \tag{2.5b}$$

The eccentricity of the streamline near (X_i, Y_i) is then $\varepsilon_i = S_i/\mu_i$ where S_i and μ_i are respectively the strain rate and the rotation rate at the vortex stagnation point. The angle Θ_i is the orientation angle of the ellipse with respect to the X-axis. It is important to point out that the 'internal' strain rate S_i is *a priori* different from the 'external' strain rate S_e estimated above. The strain rate S_e does not take into account any interaction between vorticity and strain while S_i does.

A global measure of the elliptic deformation is obtained from the second moments of the vorticity field in half a plane (see also Sipp *et al.* 2000). It requires that vorticity has not been advected or diffused across the median line between the two vortices, which is approximatively satisfied up to the merging threshold. It is also from the second moments of vorticity that a mean radius for the vortex core can be unambiguously defined whatever the vortex profile. In practice, we obtain vortex radius and vortex eccentricity by the following procedure. We choose the rotating frame such that

$$Y_c = \iint_{X>0} Y\omega \,\mathrm{d}X\,\mathrm{d}Y/\Gamma = 0,$$

which implies that the vortex centroids are located at $(\pm X_c, 0)$ with

$$X_c = \iint_{X>0} X\omega \,\mathrm{d}X\,\mathrm{d}Y/\Gamma. \tag{2.6}$$

Large and small vortex radii a_M and a_m are then defined by the formulae

$$a_M^2 = \iint_{X>0} (X(\Theta_c) - X_c)^2\omega \,\mathrm{d}X\,\mathrm{d}Y/\Gamma, \tag{2.7a}$$

$$a_m^2 = \iint_{X>0} (Y(\Theta_c))^2\omega \,\mathrm{d}X\,\mathrm{d}Y/\Gamma, \tag{2.7b}$$

where Θ_c is the orientation angle of the ellipse with respect to the X-axis based on the vorticity momentum. In particular

$$\iint_{X>0} (X(\Theta_c) - X_c)Y(\Theta_c)\omega \,\mathrm{d}X\,\mathrm{d}Y = 0. \tag{2.8}$$

It follows that the vortex radius and vortex eccentricity are defined respectively by

$$a = \sqrt{\frac{a_m^2 + a_M^2}{2}}, \tag{2.9}$$

$$\varepsilon_c = \frac{a_M - a_m}{a_M + a_m}. \tag{2.10}$$

In the following, we shall use formula (2.9) to define the vortex radius of the deformed vortex. The separation distance will be defined by $b = 2X_c$. One could have also used $b = 2X_i$ as no significant differences were observed between the positions of the vortex centres and of the stagnation points. The elliptic deformation of each vortex will be characterized by both ε_i and ε_c. These two quantities measure geometrical properties which are not necessarily related. The local eccentricity ε_i

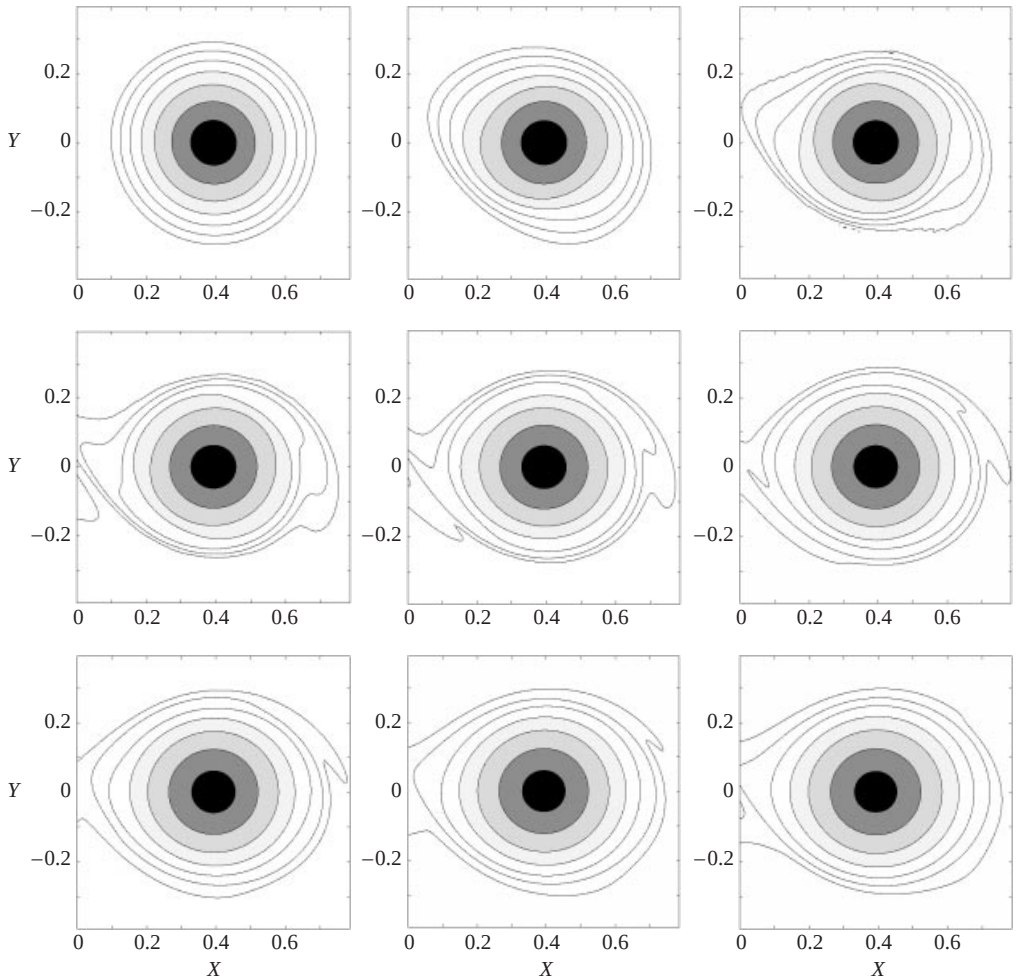

FIGURE 3. Vorticity contours during the relaxation process in the rotating frame for $n = 1$, $Re = 8000$, $a_0/b_0 = 0.1$. From right to left, top to bottom, $t\Gamma/(2\pi a_0^2) = 0 : 10 : 80$. Contours levels are $\omega/\omega_{max}(0) = 0.5, 0.1, 0.01, 0.001, 10^{-4}, 10^{-5}, 10^{-6}$.

measures the elliptic deformation of the streamline near the vortex centre while the global eccentricity ε_c measures a mean deformation of the whole vorticity region. It is useful to consider both quantities in order to identify the 'local' or 'global' nature of the dynamical evolutions described below. The local eccentricity is also interesting in itself because it measures the stability character of the vortex with respect to the tri-dimensional elliptical instability (Eloy & Le Dizès 1999; Le Dizès & Laporte 2002).

Finally, note that core deformations with larger azimuthal wavenumbers are also present but they remain small for the two-vortex system. They are not considered in the present study.

3. Relaxation processes

3.1. *Non-viscous adaptation*

The relaxation processes can be divided in two phases. The first phase is a rapid non-viscous process which consists of the adaptation of each vortex to the external

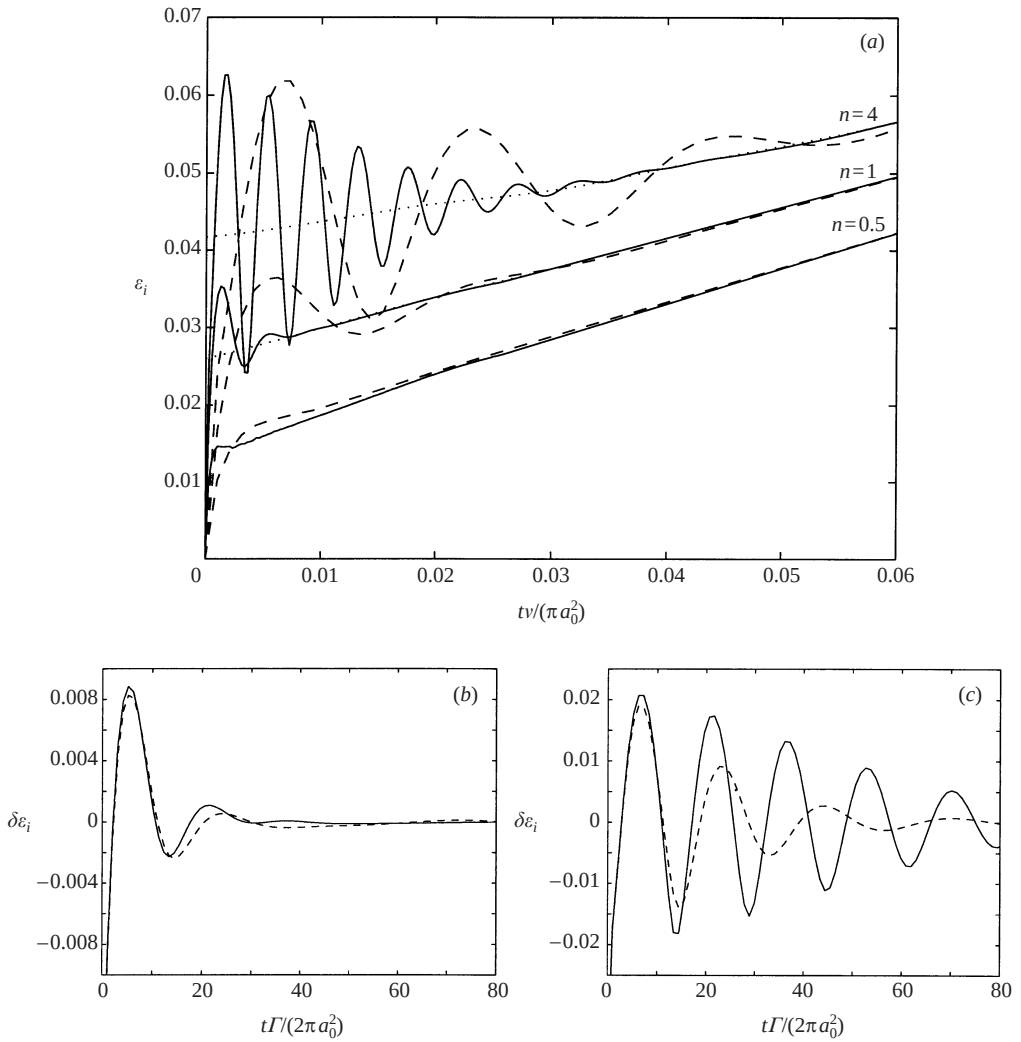

FIGURE 4. Time evolution of the local eccentricity ε_i (here $a_0/b_0 = 0.1$). Solid line: $Re = 8000$; Dashed line: $Re = 2000$. (a) Evolution on the viscous time scale for $n = 0.5, 1, 4$ and $Re = 2000, 8000$. For $n = 1$ and $n = 4$, a mean eccentricity is also indicated as dotted lines. The time evolution of ε_i around the mean eccentricity on the non-viscous time scale is shown on (b) for $n = 1$ and on (c) for $n = 4$.

field generated by the other vortex. It mostly concerns the non-axisymmetric part of the vorticity field of each vortex. An illustration of this relaxation process is provided by the snapshots of vorticity contours shown on figure 3. These snapshots show how each vortex adapts itself to the other vortex. Note, in particular, that the adaptation process is not uniform. The vortex core becomes rapidly elliptical while the very weak vorticity regions display a more complex evolution. In this section, we shall mostly focus on the deformations of the vortex core using the local and global eccentricities ε_i and ε_c.

On figures 4 and 5 are displayed, for different initial conditions, time evolutions of ε_i and ε_c respectively. Figures 4(a) and 5(b) demonstrate that both local and global eccentricities relax for all Reynolds numbers to a mean state (indicated in dotted lines)

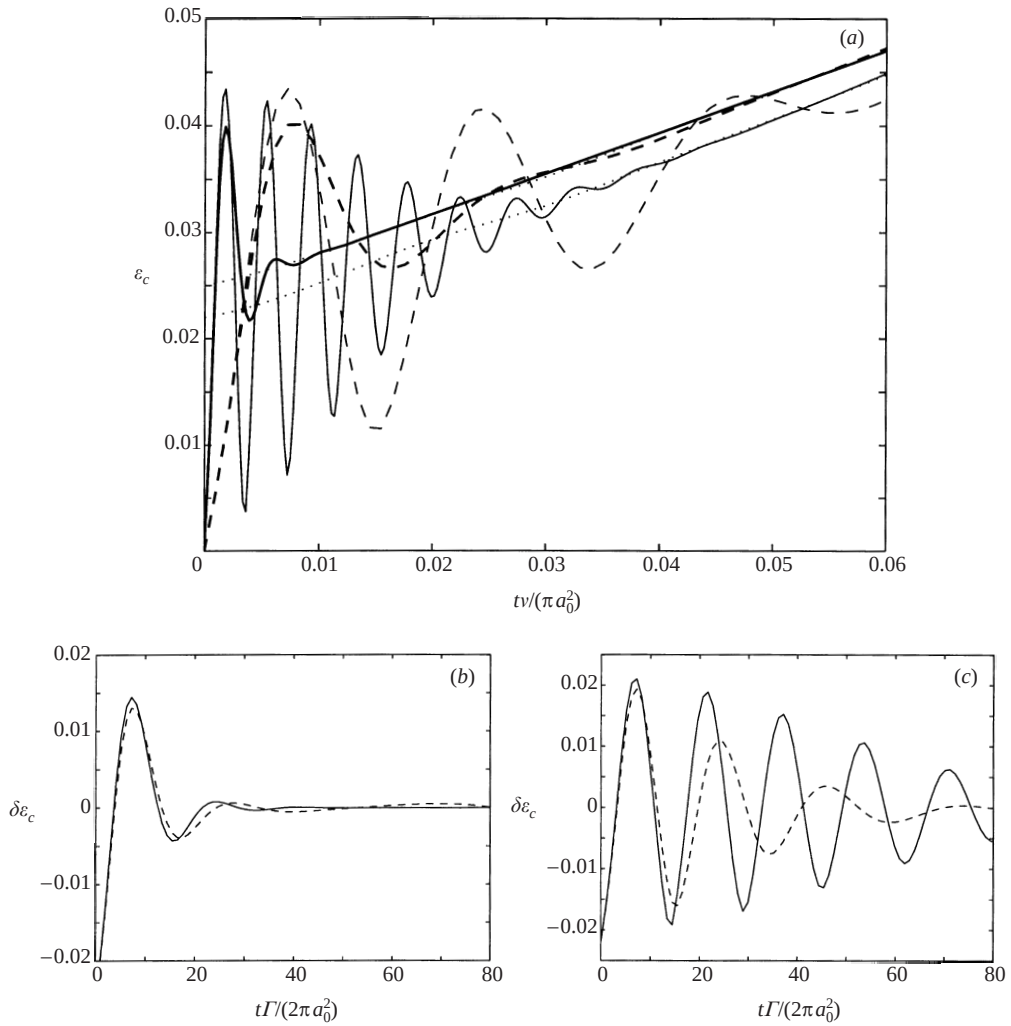

FIGURE 5. Time evolution of the global eccentricity ε_c (here $a_0/b_0 = 0.1$). Solid line: $Re = 8000$; Dashed line: $Re = 2000$. (*a*) Evolution on the viscous time scale for $n = 1$ (thick lines) and $n = 4$. and $Re = 2000, 8000$. A mean eccentricity is indicated in dotted lines for each n. The time evolution of ε_c around the mean eccentricity on the non-viscous time scale is shown on (*b*) for $n = 1$ and on (*c*) for $n = 4$.

which evolves on a viscous time scale. These mean states are different for each n but tend to converge to a unique state as time evolves. The non-viscous character of the relaxation process towards the mean state is clearly demonstrated on figures 4(b, c) and 5(b, c) where the fluctuations $\delta\varepsilon_i$ and $\delta\varepsilon_c$ around the mean eccentricity are plotted versus a non-viscous time scale. These figures show the following features:

(*a*) The relaxation process takes a longer time for steeper profiles. In particular, eccentricity oscillates strongly around the mean for $n = 4$ whereas there is no oscillation for $n = 0.5$ and only weak oscillations for $n = 1$.

(*b*) There is a weak Reynolds number dependence of the process for non-Gaussian profiles. The relaxation process is more rapid (on a non-viscous time scale) for larger Reynolds number when the profile is steep ($n > 1$) while it is the opposite when the profile is flat ($n < 1$).

(*c*) Relaxation processes towards a mean state are similar for the global and the local eccentricity.

Note however, that the dependence of mean eccentricity on n is clearly different for local and global quantities: the mean value of the global eccentricity ε_c slightly increases with n whereas the mean value of the local eccentricity ε_i decreases with n.

The features pointed out above can be explained by considering the evolution of linear elliptic perturbations on a single quasi-stationary vortex. *A priori*, this vortex would be the slightly deformed vortex towards which each core relaxes on the non-viscous time scale. But for the ratio a/b under consideration ($a/b \approx 0.1$), the deformation is small; the linear perturbations are therefore expected to be close to those of the underlying axisymmetric vortex.

Results concerning the time evolution of linear perturbations in the large Reynolds number limit were recently obtained by Bernoff & Lingevitch (1994), Bassom & Gilbert (1998, 1999), Schecter *et al.* (2000) and Balmforth *et al.* (2001) among others. Bassom & Gilbert (1998, 1999) obtained a non-viscous asymptotic solution for the elliptic perturbations which exhibits an algebraically decreasing behaviour in time. Schecter *et al.* (2000) demonstrated that in the inviscid limit a damped 'quasi-mode' was also excited during the transient. This 'quasi-mode' is singular in a non-viscous flow. In a viscous flow, it is however a regular linear normal mode as viscosity smooths the singularity. Interestingly, the damping rate of this mode is not dependent on viscosity for large Reynolds numbers and is the same as that of the quasi-mode. By contrast, the asymptotic solution of Bassom & Gilbert (1998) is corrected in the viscous regime by damping factors which are strongly dependent on both the Reynolds number and the position (see Lundgren 1982; Bajer, Bassom & Gilbert 2001).

Here we argue that the relaxation phenomenon of the vortex core is the signature of the linear normal mode. This would in particular explain the above statement (*c*). Moreover, as we shall now show, the normal mode characteristics are also compatible with figures 4 and 5. For large Reynolds numbers, Le Dizès (2000) obtained the complex frequency of such a mode for a family of vortex profiles ranging from Rankine (top-hat) to Gaussian. He showed that the steeper the profile the weaker the damping of the mode in agreement with an early result by Briggs, Daugherty & Levy (1970) for inviscid quasi-modes. Such a characteristic qualitatively agrees with statement (*b*). For a Gaussian profile, Le Dizès (2000) also obtained a theoretical value for the complex frequency $\omega_g/\Omega(0) = 0.22 - 0.08\mathrm{i}$ ($\Omega(0)$ is the angular velocity at the vortex centre) which is within 5% of the values measured from figures 4(*b*) and 5(*b*). This confirms that even for such a large damping, the relaxation process is governed by the linear mode. For a non-Gaussian profile, figures 4(*c*) and 5(*c*) clearly show that both the real frequency and the damping rate of the relaxation oscillations vary as time evolves. Figure 6 demonstrates that this variation is associated with the viscous modification of the underlying axisymmetric profile. On that figure are plotted as a function of a viscous time scale, the local frequency and the local damping rate of the relaxation oscillations for $n = 4$ and $Re = 2000$, 4000, 8000, 16 000. Frequencies are obtained from the distance between consecutive peaks, or consecutive zeros, while damping rates are obtained from amplitude ratios between consecutive peaks. For small Reynolds numbers, the error bars are large. Yet, the results displayed in figure 6 are sufficiently convincing to suggest the following assertion: both frequencies and damping rates for all the Reynolds numbers we have considered can be superimposed on a same curve which tends for large time to the prediction for a Gaussian vortex.

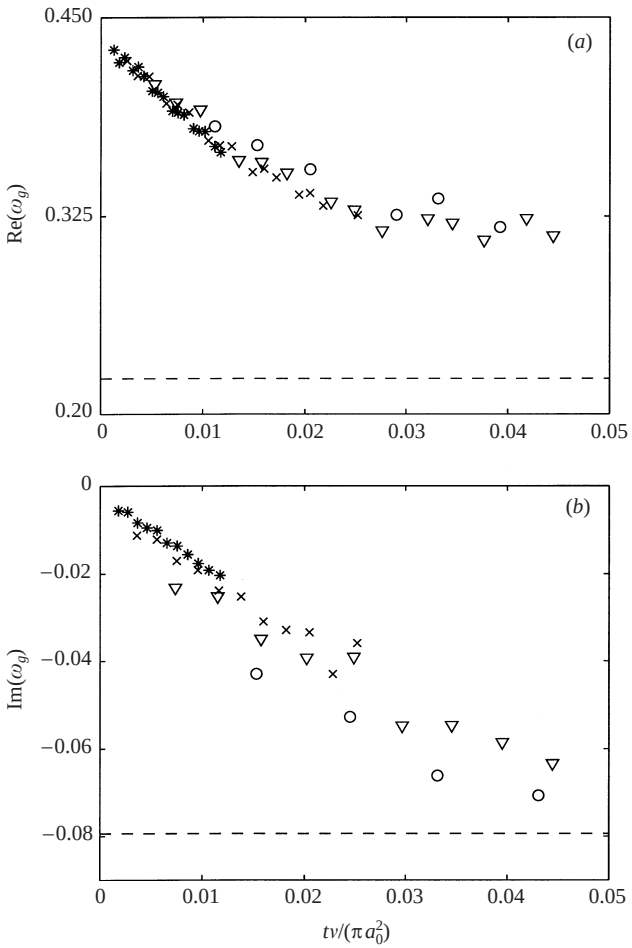

FIGURE 6. Time evolution of the (local) frequency (*a*) and damping rate (*b*) of the local eccentricity ε_i around its mean value on a viscous time scale for $n = 4$ and $Re = 16\,000$ (stars), $Re = 8000$ (crosses), $Re = 4000$ (triangles), $Re = 2000$ (circles). Both frequency and damping rate are normalized by the angular velocity in the vortex centre (half of the vorticity maximum). The dashed line is the linear non-viscous prediction for a Gaussian profile.

This is in agreement with the scenario we have already mentioned: the first rapid phase of the relaxation process is non-viscous and only dependent on the underlying vorticity profile. The weak dependence on the Reynolds number is associated with the modification of the vorticity profile by viscous diffusion. As expected, such a dependence is present for $n = 4$ but not for $n = 1$. The convergence for large time towards the Gaussian prediction results from the second relaxation process, which is discussed in the next section.

Before moving on to that point, it is worth mentioning that the relaxation process had already been observed in the non-viscous response of a Gaussian vortex to a pure external strain field (Bassom & Gilbert 1999). This process, denoted the 'rebound phenomenon' was erroneously attributed to the inertial spiral structure of the vortex response. Comparisons of the frequency and damping rate of this rebound phenomenon could easily demonstrate that it is instead associated with the damped quasi-mode obtained by Schecter *et al.* (2000). Sipp *et al.* (2000) also noticed the

relaxation phenomenon in the case of two counter-rotating vortices. They reached, for Rankine vortices, conclusions similar to ours: the oscillations are due to a two-dimensional Kelvin mode of the vortex. Note however, that for Rankine vortices or other vortices with vorticity confined in a finite area the Kelvin modes are neutral (for large Reynolds number). Undamped oscillations are then expected to be seen as long as the vorticity profile has not been sufficiently modified by viscosity (Melander *et al.* 1988).

3.2. *Viscous diffusion*

The second relaxation process occurs on a viscous time scale. In Sipp *et al.* (2000), it was observed that for counter-rotating vortices this process is a viscous attracting phenomenon. Whatever the initial vorticity profile, the solution tends to relax to a unique state which seems to be independent of the Reynolds number. As we shall see in this section, a similar conclusion is reached for co-rotating vortices. Here, however, we go one step further by characterizing the viscous process. We demonstrate that it is very close to the viscous relaxation of any axisymmetric vortex to a Gaussian. In § 5, a few differences are also pointed out.

The time evolution of the vorticity field for a single axisymmetric vortex is given exactly by a diffusion equation. This property guarantees that the Gaussian vorticity profile is a global attractor for all the axisymmetric vortices. Moreover, the Gaussian vortex has a self-similar evolution which conserves its profile. It has a vorticity maximum which is given for any time by $\omega_{max} = \Gamma/(\pi a^2)$. For the family of profiles (2.2), such a relation is satisfied for the Gaussian vortex ($n = 1$) only. On the other hand, the radius a always evolves according to $a = \sqrt{a_0^2 + 4\nu t}$ whatever the profile and this evolution is also valid for a non-axisymmetric vortex as long as a is defined by (2.9) (Batchelor 1967). This property implies that as long as the merging process has not started (that is, b has not started to decrease), plotting a quantity versus a viscous time scale is equivalent to plotting this quantity versus a/b.

On figure 7(a) is plotted the evolution of $\omega_{max}\pi a^2/\Gamma$ as a function of a/b for several initial conditions with different vorticity profiles. For each initial condition, the evolution both for the two-vortex system and for a single vortex is represented. Figure 7 clearly shows that the viscous diffusion of each vortex is not affected by the other vortex: it is therefore given by a simple diffusion equation. As a consequence, there should be no Reynolds number dependence of the relaxation process on a viscous time scale, or equivalently if plotted as a function of a/b. Here, this has been checked for Reynolds number ranging between 500 and 8000.

For the same initial conditions as above, the angular frequency of the vortex system normalized by the vorticity maximum is plotted on figure 7(b). This quantity is compared to a 'single vortex' estimate, obtained by taking for the angular frequency the two-point-vortex value: $\mathrm{d}\Theta/\mathrm{d}t = \Gamma/(\pi b^2)$. The good agreement between both quantities demonstrates that the two-point vortex model plus a simple diffusion of the profile, as if the vortex were alone, provide an excellent model for both the angular frequency and the vorticity maximum. Again, no dependence on the Reynolds number has been noticed.

As for counter-rotating vortices (Slipp *et al.* 2000), these results lead us to put forward the following assertions:

(a) Before merging, there exists a unique attractive solution for the two-co-rotating vortex system.

(b) This solution is parametrized by a single parameter a/b. It can be obtained from an initial condition with a Gaussian profile.

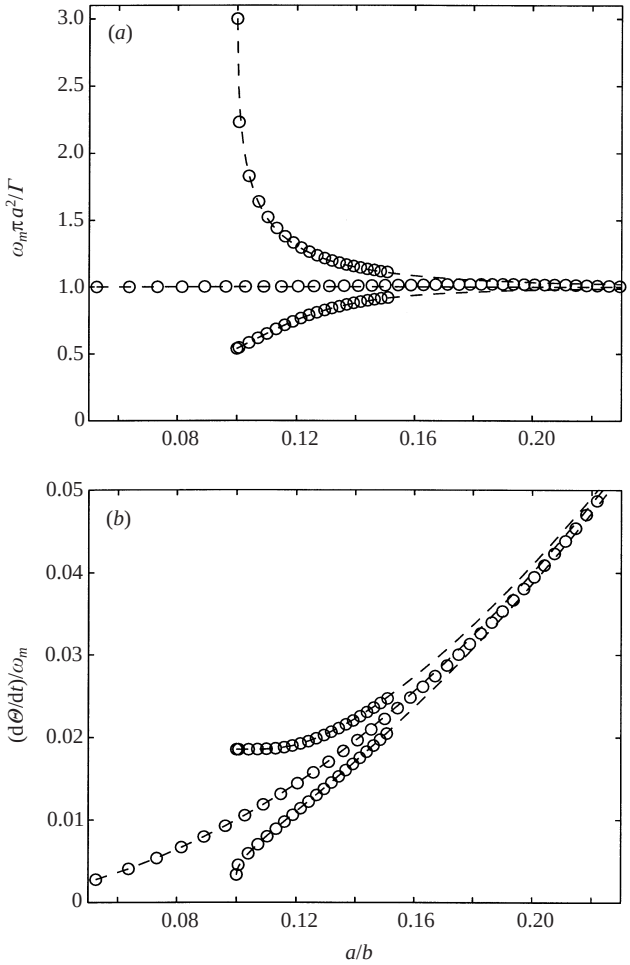

FIGURE 7. Normalized vorticity maximum (a) and angular velocity (b) as a function of a/b for three different initial conditions. Circles: evolution for the two-vortex system. Dashed lines: evolution for a single vortex. In (b), $d\Theta/dt$ is given by the two-vortex model $d\Theta/dt = f = \Gamma/(\pi b^2)$ for the single vortex, while it is directly calculated from the simulation for the two-vortex system.

(c) There is no visible Reynolds number dependence of the vortex core properties in the range $Re = 500$–8000.

Other characteristics of the attractive solution are given in the next section. As for the vorticity maximum and the angular velocity of the vortex system, we have not noticed any significant dependence on the Reynolds number for these quantities.

4. Other characteristics of the attractive solution

In this section, other properties of the attractive solution are provided for a/b ranging from 0.05 to 0.22. These properties are obtained from a single simulation by letting two Gaussian vortices evolve with sufficiently small initial a_0/b_0. The ratio a/b increases progressively due to viscous diffusion and covers all the range $a_0/b_0 < a/b < 0.22$ up to the merging process. Here, we have chosen $a_0/b_0 = 0.05$ and $Re = 2000$.

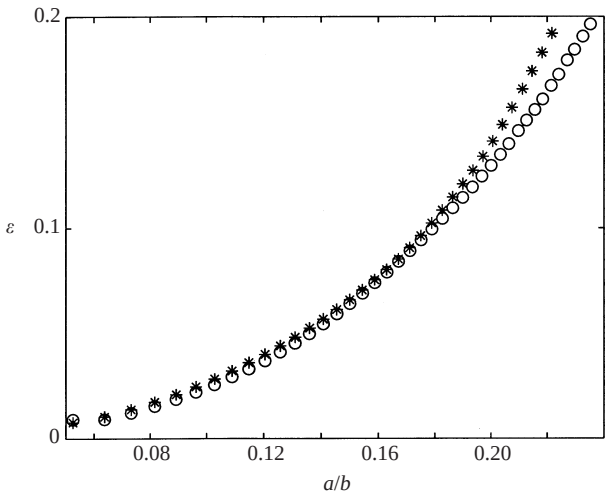

FIGURE 8. Local eccentricity ε_i (*) and global eccentricity ε_c (○) versus a/b for the attractive solution. Data are obtained from the evolution of two Gaussian profiles ($n = 1$) at $a_0/b_0 = 0.05$ with $Re = 2000$.

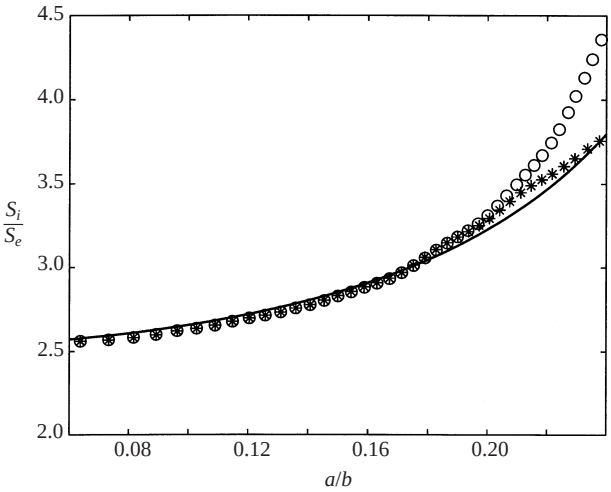

FIGURE 9. Strain rate in the centre of one vortex, normalized either by $\Gamma/(2\pi b_0^2)$ (*) or by $\Gamma/(2\pi b^2)$ (○). Solid line: theoretical prediction obtained from the analysis of a single Gaussian vortex in a normalized strain field rotating at the angular frequency of the vortex pair (Le Dizès 2000).

On figure 8 are displayed the two quantities which were used above to characterize the elliptical deformation of each vortex core. As expected, local and global eccentricities grow in the same fashion as a/b increases. However, the two quantities depart from each other when a/b reaches approximately 0.18. The global eccentricity then tends to grow more slowly. This departure is probably associated with the finite size of the vortex. As the global eccentricity is an average measure of the deformation, it may differ from its estimate in the vortex centre when the deformation is no longer uniform.

On figure 9 is plotted the strain rate at the vortex stagnation point normalized by either $\Gamma/(2\pi b^2)$ or $\Gamma/(2\pi b_0^2)$. The latter quantities can be considered as external

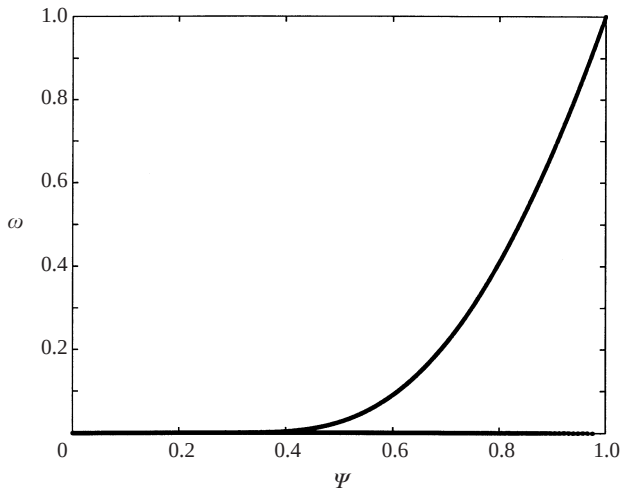

FIGURE 10. Typical scatter plot (Ψ, ω) for small a/b (here, $a/b \approx 0.14$, $Re = 2000$, $n = 1$).

strain rates as they correspond to the strain rates induced by a point vortex of circulation Γ located at a distance b and b_0 respectively. The first normalization takes into account the variation of the separation distance b while the second does not. Figure 9 therefore displays the ratio S_i/S_e between internal and external strain rates. This ratio was also computed by Le Dizès (2000) in the ideal configuration of a single vortex in an external rotating strain field. He demonstrated that, in the limit of large Reynolds number and weak external strain rate S_e, the ratio S_i/S_e is a function of the angular frequency and of a parameter $h = 1/(ReS_e^{3/2})$ which measures the nonlinear interaction between strain and vorticity. Here the dependence on h is negligible because the angular frequency (approximately $(a/b)^2$) remains smaller than 0.06 (see Le Dizès 2000). The theoretical curve is plotted as a solid line on figure 9. The agreement between the theory and the numerics is remarkably good up to $a/b \approx 0.18$. For $0.18 < a/b < 0.22$, the theory slightly underestimates the strain rate in the vortex centre but remains within 3% of the numerics. Above $a/b \approx 0.22$, the merging process is active: b starts to decrease. The two numerical results depart from each other as the normalizations are now different.

After the first non-viscous relaxation process, the vortex system stops evolving on a non-viscous time scale. At leading order, one therefore expects the two vortices to be, in the rotating frame, close to a stationary solution of the Euler equation. This is confirmed by the scatter plot of vorticity versus streamfunction shown on figure 10. Indeed, before merging, all the (vorticity, streamfunction) points align on a single curve which proves that there is indeed a functional relation between ω and Ψ. This shows that the rotating system is close to a stationary solution of the Euler equation. Note however that this result mostly concerns regions of strong vorticity. In the next section, we shall see that a weak time dependence is present in regions far from the vortices.

Scatter plots were also used by Sipp *et al.* (2000) for counter-rotating vortices. For small a/b and Gaussian profiles, they obtained vorticity, streamfunction) relations which look similar to ours. This is not surprising as one could check that the simple sum of two Gaussian vortices also provides a functional relation of the same type.

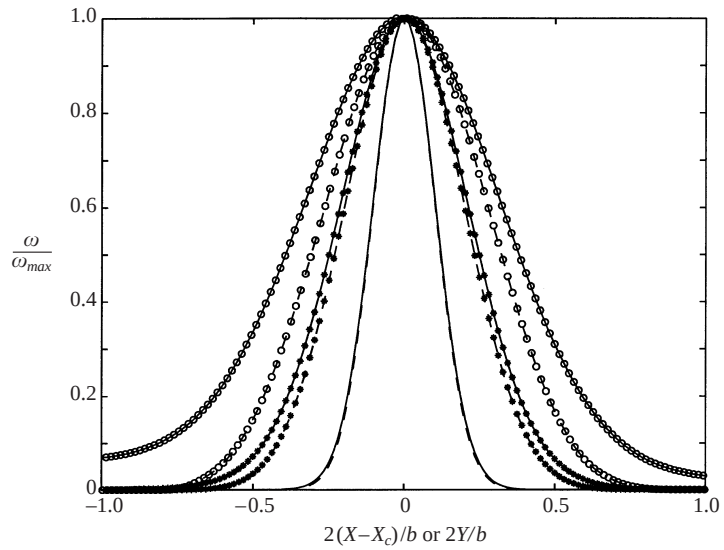

FIGURE 11. Normalized vorticity profiles for different values of a/b. The profiles are taken along two lines centred on the vorticity maximum: the line connecting the two vortex centres (solid line), and the line perpendicular to it (dashed line). Lines without symbols: $a/b = 0.07$; $*$, $a/b = 0.13$; $\circ$, $a/b = 0.18$.

On figure 11 are displayed vorticity profiles in the vortex core for different values of a/b along the line connecting the two vortex centroids and that perpendicular to it. On these plots are clearly seen the vortex core deformations as a function of a/b: profiles are wider along the centrelines and the difference increases as a/b increases. Note also the visible asymmetry of the wider profile: this is due to an accumulation of vorticity at the central hyperbolic point which is located at $2(X - X_c)/b = -1$ on figure 11 (see next section).

5. Reynolds number dependence

The Reynolds number dependence of the attractive solution is weak and becomes increasingly weaker with smaller a/b. However, this dependence exists and can be quantified if one looks at particular regions where it is strongest. These regions can be easily identified on the typical streamline pattern shown on figure 2. This pattern, drawn here for a small a/b and a particular value of the Reynolds number, is almost independent of a/b and viscosity. It can be used in the present discussion for all a/b and Reynolds numbers we have considered. In particular, one sees on figure 2 that the streamline pattern possesses hyperbolic points and separatrices connecting these points which go to regions far away from the vortices. It is in the neighbourhood of these separatrices that the Reynolds number dependence is the strongest. On figure 12(a, b) are plotted vorticity contours for two configurations with the same a/b obtained from the same initial condition but with different *Re*. It is clearly seen that the vortex core in the configuration with the largest Reynolds number has lost more vorticity into the arms connecting both external hyperbolic points. The presence of vorticity arms (or filaments) is the manifestation of the so-called stripping or erosion process (Legras & Dritschel 1993; Mariotti, Legras & Dritschel 1994). As explained by Legras & Dritschel (1993), this phenomenon is due to the advection of vorticity

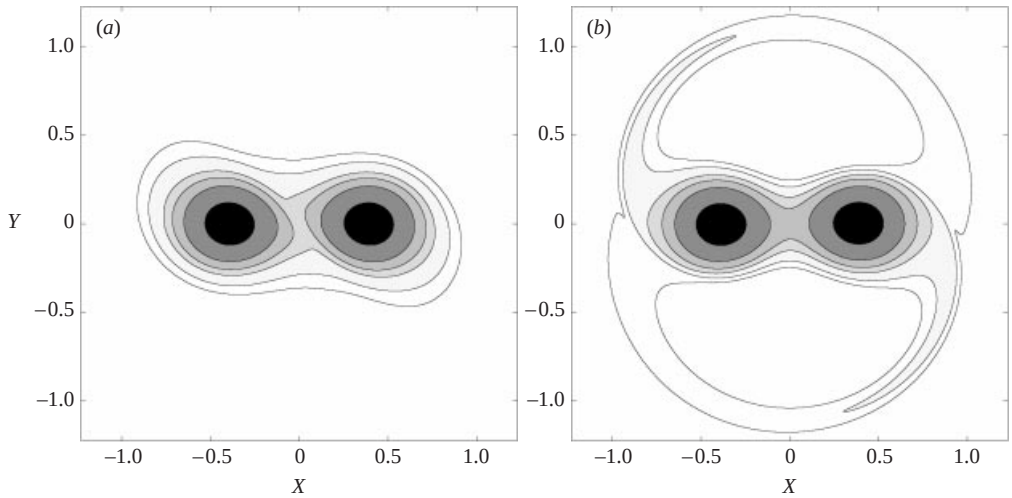

FIGURE 12. Vorticity levels for $a/b \approx 0.2$ for two simulations started from $a_0/b_0 = 0.05$ and $n = 1$ but different Reynolds numbers: (*a*) $Re = 500$; (*b*) $Re = 8000$. Contours levels are $\omega/\omega_{max} = 0.5$, 0.1, 0.03, 0.01, 0.001, 0.0001.

along streamlines that leave the vortex core. It leads to an 'erosion' of the vortex and a steepening of the transverse vorticity profile. For the streamline pattern shown on figure 2, erosion first occurs on separatrices connected to the hyperbolic points as they are the closest separatrices to the vortex centre that leave it. Vorticity is thus shed away from the vortex through both external hyperbolic points. Although viscosity intervenes in the complex advection–diffusion process near the hyperbolic points, one expects vorticity to be advected in the arms on a non-viscous time scale. In particular, one expects erosion to occur on a faster time scale than the viscous radial diffusion of the vortex. This implies that for two systems which have evolved on the same viscous time interval (as it is the case for the configurations shown on figure 12), erosion has been more important in the system with the largest Reynolds number. This is qualitatively in agreement with the pictures of figure 12.

It is also interesting to note on figure 12 that more vorticity is present in the central hyperbolic point in the largest Reynolds number configuration. This dependence on the Reynolds number is quantified on figure 13, where three evolutions starting from the same initial condition ($n = 1$, $a_0/b_0 = 0.05$) with different Reynolds numbers are shown. The collapse of these on a single curve demonstrates that in the range of Reynolds number we have considered, vorticity at the central hyperbolic point evolves according to a simple law of the form $\omega(0) = Re^{1/3} f(a/b)$. This scaling can probably be attributed to the shear-diffusion of vorticity during its advection. Indeed, it is well-known that the cross-stream diffusion of a passive scalar in a shear flow is on a time scale of order $Re^{1/3}$ (Rhines & Young 1983) which could explain the appearance of the factor $Re^{1/3}$. However, here the situation is not as simple as in Rhines & Young (1983) because along the separatrix connecting stagnation points, the diffusion properties are actually different as explained by Lingevitch & Bernoff (1994). The justification of the scaling is therefore not straightforward and we leave it for the future.

It is worth pointing out that the time-dependent effects identified in this section are limited to specific regions located outside the vortex core. For small a/b, they concern very small levels of vorticity which make them almost invisible on global

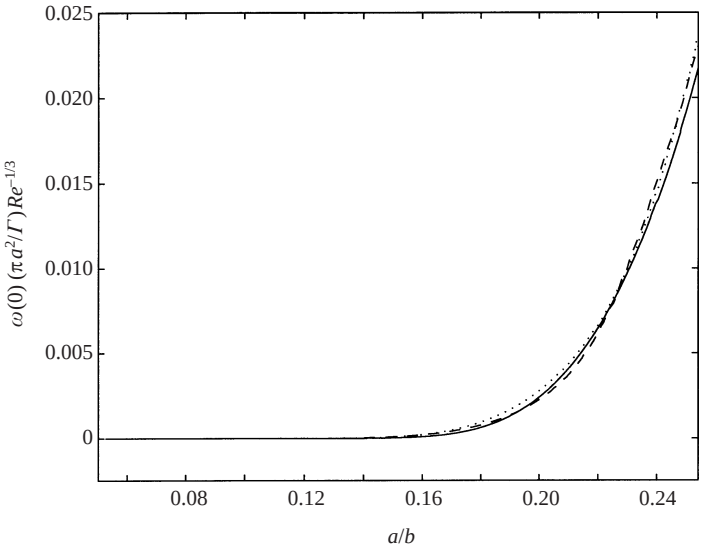

FIGURE 13. Vorticity at the central hyperbolic point, rescaled by a $Re^{-1/3}$ factor versus a/b for three simulations starting from the condition $a_0/b_0 = 0.05$, $n = 1$ but different Reynolds numbers. Solid, dotted and dashed lines correspond to $Re = 500$, 2000 and 8000 respectively.

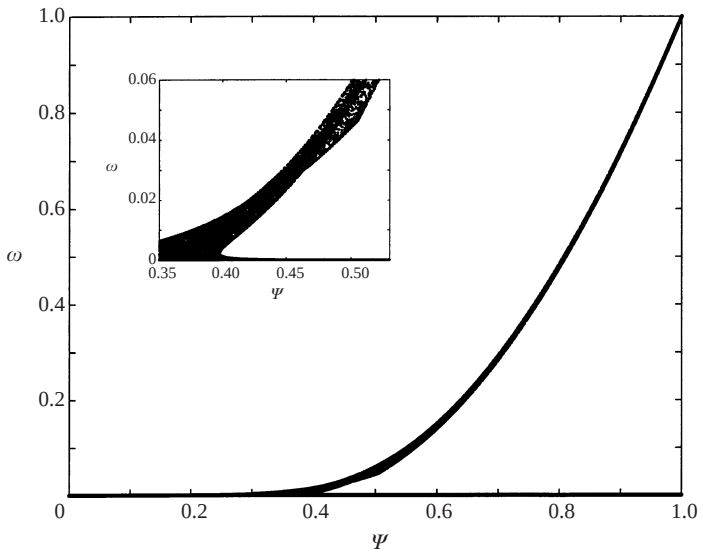

FIGURE 14. Scatter plot (Ψ, ω) close to the merging threshold (here, $a/b \approx 0.21$, $Re = 2000$, $n = 1$). The close-up view shows the thickening of the functional relation between Ψ and ω for the small vorticity levels: the thicker regions correspond to the neighbourhoods of the hyperbolic points.

(Ψ, ω) scatter plots like the one shown on figure 10. However, very close to the merging threshold ($a/b \approx 0.22$), these effects can become sufficiently important to become visible on scatter plots (see figure 14). They are associated with a thickening of the functional relation close to particular points which correspond to the regions mentioned above (separatrix connecting hyperbolic stagnation points).

6. Conclusion

In this paper, the viscous interactions of two identical vortices have been analysed before the merging threshold is reached. Two relaxation processes have been identified. The first one is a non-viscous adaptation of each vortex with respect to the other which results from the fact that the initial condition (i.e. the sum of two axisymmetric vortices) is not a solution of the Navier–Stokes equation. We have demonstrated that both the eccentricity of the streamlines near each vortex centre and the eccentricity of each vortex core rapidly relax with an oscillating behaviour to a non-zero value. This oscillating behaviour has been related to a damped linear mode of the vortex. For a Gaussian vorticity profile, both the damping rate and the frequency of the elliptic deformation have been shown to correspond to the characteristics of the linear mode obtained by Le Dizès (2000). For steeper vorticity profiles, the damping rate of the oscillations has been found to be smaller, in agreement with previous results (Briggs *et al.* 1970; Le Dizès 2000). These findings imply that the characteristics of the first relaxation process are only dependent on the vorticity profile of each vortex. This means that there is no significant dependence on the Reynolds number apart from the dependence via the modification of the vorticity profile due to viscous diffusion. In particular, for the Gaussian profile, which is not affected by viscosity, time evolutions of the elliptic deformations on a non-viscous time scale have been demonstrated to be rigorously identical for all the Reynolds number range $Re = 500$–$16\,000$. Whatever the profile, the first relaxation process leads to a state where each vortex is slightly deformed by the field generated by the other vortex. As long as a/b is small, this state remains quasi-steady in a rotating frame and evolves due to viscous diffusion. This constitutes the second viscous relaxation process. We have demonstrated that the viscous diffusion of the two-vortex system is very similar to the simple diffusion of a single axisymmetric vortex. This has lead us to the following conjecture: as all axisymmetric vortices relax towards a Gaussian vortex, two-vortex systems also relax to a unique state which corresponds to the vortex system with Gaussian profiles. This state can be parametrized by a single parameter a/b. A similar conclusion was previously reached for counter-rotating vortices by Sipp *et al.* (2000).

An important part of the paper has been concerned with the characterisation of this attractive state. We have demonstrated that the elliptic deformation of the vortices can be captured by a simplified model in which the deformation is assumed to be generated by a uniform rotating external strain field. Using for the strain rate and the angular frequency of the external field values predicted by the two-point-vortex model, we have obtained a very good estimate for the strain rate in the vortex centre for vortices satisfying $a/b < 0.18$. A similar model was used in Jiménez *et al.* (1996) to analyse the elliptic deformation of vortices encountered in two-dimensional turbulence. Without considering the effects of rotation, they showed that the model provides, at least in a statistical sense, a good description of the vortex deformation. Here, the comparison is much more precise and takes into account rotation which is known to modify the elliptic deformation characteristics (Le Dizès 2000). The good agreement constitutes an interesting result which could be very useful in the context of the elliptical instability as it may provide a simple way to obtain the stability characteristics of a vortex pair (Le Dizès & Laporte 2002).

A weak dependence on the Reynolds number has been observed in the characteristics of the attractive solution. This implies that the viscous relaxation of a two-vortex system cannot be perfectly identical to the relaxation of a single axisymmetric vortex in which no Reynolds number dependence is present. The regions where the Reynolds

number dependence is the most apparent have been identified as the neighbourhood of the separatrices connected to the hyperbolic points. In these regions, complex advection–diffusion mechanisms are expected to be present on a time scale intermediate between the turn-over time and the viscous time associated with radial diffusion as is the case for a passive scalar (Rhines & Young 1983; Lingevitch & Bernoff 1994). They can also be linked to the so-called stripping or erosion processes which have been phenomenologically described in several works (see for instance Legras & Dritschel 1993; Mariotti *et al.* 1994).

A particular Reynolds number behaviour in $Re^{1/3}$ has also been obtained for the evolution of the vorticity amplitude at the central hyperbolic point. This scaling has been observed in the whole range of Reynolds numbers we have considered, that is $Re = 500$–8000. However, one has to keep in mind that the peak of vorticity is bounded by its initial value. For a given a/b, this scaling should therefore break down for sufficiently large Reynolds numbers. If a stationary state is reached at the limit of infinite Reynolds numbers, one would expect the hyperbolic point vorticity to saturate to the mean vorticity along the whole separatrix connected to that point. Further studies are however needed to clarify this issue, in particular to determine whether a stationary state is reached in the limit $Re \to \infty$ at the hyperbolic point.

The results obtained in this paper also have implications for the merging process which starts when a/b has reached a sufficiently large value. This process is characterized by the rapid displacement of the vortices towards each other which leads to the formation of a single vortex on a non-viscous time scale. Here, because of viscosity which makes the ratio a/b grow in time, merging always occurs without the need of a third vortex (Kevlahan & Farge 1997) or an additional strain field. Merging is often interpreted as the dynamical behaviour resulting from a non-viscous instability of the vortex pair (Dritschel 1985). Recent work by Meunier *et al.* (2002) demonstrated that this interpretation could provide an estimate for the merging threshold which is in agreement with experiments (Meunier & Leweke 2001). The critical ratio $a/b \approx 0.22$ obtained here for the attractive solution (with Gaussian vortices) also agrees with the experiments.

However, the Reynolds dependence of the merging threshold remains to be addressed. For $Re = 500$–8000, a weak dependence has been observed due to the erosion of the vortices through the hyperbolic points of the streamline pattern. Although we have not noticed any significant modifications in the merging threshold in this range, this erosion process could have a measurable effect for very large Reynolds numbers.

REFERENCES

Agullo, O. & Verga, A. 2001 Effect of viscosity in the dynamics of two point vortices: Exact results. *Phys. Rev.* E **63**, 056304–1–14.

Bajer, K., Bassom, A. P. & Gilbert, A. D. 2001 Accelerated diffusion in the centre of a vortex. *J. Fluid Mech.* **437**, 395–411.

Balmforth, N. J., Llewellyn Smith, S. G. & Young, W. R. 2001 Disturbing vortices. *J. Fluid Mech.* **426**, 95–133.

Basdevant, C., Legras, B., Sadourny, R. & Bérland, M. 1981 A study of barotropic model flows: intermittency, waves and predictability. *J. Atmos. Sci* **38**, 2305–2326.

Bassom, A. P. & Gilbert, A. D. 1998 The spiral wind-up of vorticity in an inviscid planar vortex. *J. Fluid Mech.* **371**, 109–140.

Bassom, A. P. & Gilbert, A. D. 1999 The spiral wind-up and dissipation of vorticity and a passive scalar in a strained planar vortex. *J. Fluid Mech.* **398**, 245–270.

Batchelor, G. K. 1967 *An Introduction to Fluid Dynamics*. Cambridge University Press.

Bernoff, A. J. & Lingevitch, J. F. 1994 Rapid relaxation of an axisymmetric vortex. *Phys. Fluids* **6**, 3717–3723.

Brandt, S. A. & Iversen, J. D. 1977 Merging of aircraft trailing vortices. *J. Aircraft* **14**, 1212–1220.

Briggs, R. J., Daugherty, J. D. & Levy, R. H. 1970 Role of landau damping in cross-field electron beams and inviscid shear flow. *Phys. Fluids* **13**, 421–432.

Carnevale, G. F., McWilliams, J. C., Pomeau, Y., Weiss, J. B. & Young, W. R. 1991 Evolution of vortex statistics in two-dimensional turbulence. *Phys. Rev. Lett.* **66**, 2735–2738.

Carnevale, G. F., McWilliams, J. C., Pomeau, Y., Weiss, J. B. & Young, W. R. 1992 Rates, pathways, and end states of nonlinear evolution in decaying two-dimensional turbulence: Scaling theory versus selective decay. *Phys. Fluids* A **4**, 1314–1316.

Couder, Y. 1983 Observation expérimentale de la turbulence bidimensionnelle dans un film liquide mince. *C. R. Acad. Sci. Paris* II **297**, 641–645.

Dritschel, D. G. 1985 The stability and energetics of corotating uniform vortices. *J. Fluid Mech.* **157**, 95–134.

Dritschel, D. G. & Waugh, D. W. 1992 Quantification of the inelastic interaction of unequal vortices in two-dimensional vortex dynamics. *Phys. Fluids* A **4**, 1737–1744.

Ehrenstein, U. & Rossi, M. 1999 Equilibria of corotating nonuniform vortices. *Phys. Fluids* **25**, 3416–3425.

Eloy, C. & Le Dizès, S. 1999 Three-dimensional instability of Burgers and Lamb–Oseen vortices in a strain field. *J. Fluid Mech.* **378**, 145–166.

Jiménez, J., Moffatt, H. K. & Vasco, C. 1996 The structure of the vortices in freely decaying two dimensional turbulence. *J. Fluid Mech.* **313**, 209–222.

Kevlahan, N. K.-R. & Farge, M. 1997 Vorticity filaments in two-dimensional turbulence: creation, stability and effect. *J. Fluid Mech.* **346**, 49–76.

Le Dizès, S. 2000 Non-axisymmetric vortices in two-dimensional flows. *J. Fluid Mech.* **406**, 175–198.

Le Dizès, S. & Laporte, F. 2002 Theoretical predictions for the elliptic instability in a two-vortex flow. *J. Fluid Mech.* (in press).

Legras, B. & Dritschel, D. G. 1993 Vortex stripping and the generation of high vorticity gradients in two-dimensional flows. *Appl. Sci. Res.* **51**, 445–455.

Lingevitch, J. F. & Bernoff, A. J. 1994 Advection of a passive scalar by a vortex couple in the small-diffusion limit. *J. Fluid Mech.* **270**, 219–249.

Lingevitch, J. F. & Bernoff, A. J. 1995 Distortion and evolution of a localized vortex in an irrotational flow. *Phys. Fluids* **7**, 1015–1026.

Lundgren, T. S. 1982 Strained spiral vortex model for turbulent fine structure. *Phys. Fluids* **25**, 2193–2203.

Mariotti, A., Legras, B. & Dritschel, D. G. 1994 Vortex stripping and the erosion of coherent structures in two-dimensional flows. *Phys. Fluids* A **6**, 3954–3962.

McWilliams, J. C. 1984 The emergence of isolated coherent vortices in turbulent flow. *J. Fluid Mech.* **146**, 21–43.

McWilliams, J. C. 1990 The vortices of two-dimensional turbulence. *J. Fluid Mech.* **219**, 361–385.

Melander, M. V., Zabusky, N. J. & McWilliams, J. C. 1988 Symmetric vortex merger in two-dimensions: causes and conditions. *J. Fluid Mech.* **195**, 303–340.

Meunier, P., Ehrenstein, U., Leweke, T. & Rossi, M. 2002 A merging criterion for two-dimensional co-rotating vortices. *Phys. Fluids* **14**, 2757–2766.

Meunier, P. & Leweke, T. 2001 Three-dimensional instability during vortex merging. *Phys. Fluids* **13**, 2747–2750.

Moore, D. W. & Saffman, P. G. 1971 Structure of a line vortex in an imposed strain. In *Aircraft Wake Turbulence* (ed. R. Olsen, G. Golburg, M. M. Rogers), pp. 339–354. Plenum.

Overman, E. A. & Zabusky, N. J. 1982 Evolution and merger of isolated vortex structures. *Phys. Fluids* **25**, 1297–1305.

Rhines, P. B. & Young, W. R. 1983 How rapidly is a passive scalar mixed within closed streamlines? *J. Fluid Mech.* **133**, 133–145.

Saffman, P. G. 1992 *Vortex Dynamics*. Cambridge University Press.

Saffman, P. G. & Szeto, R. 1980 Equilibrium of a pair of equal uniform vortices. *Phys. Fluids* **23**, 2339–2342.

Schecter, D. A., Dubin, D. H. E., Cass, A. C., Driscoll, C. F., Lansky, I. M. & O'Neil, T. M. 2000 Inviscid damping of asymmetries on a two-dimensional vortex. *Phys. Fluids* **12**, 2397–2412.

Sipp, D., Jacquin, L. & Cossu, C. 2000 Self-adaptation and viscous selection in concentrated two-dimensional dipoles. *Phys. Fluids* **12**, 245–248.

Winant, C. D. & Browand, F. K. 1974 Vortex pairing: the mechanism of turbulent mixing-layer growth at moderate reynolds number. *J. Fluid Mech.* **63**, 237–255.